Petroleum Research 7 (2022) 62–76

Contents lists available at ScienceDirect

Petroleum Research

journal homepage: http://www.keaipublishing.com/en/journals/petroleum-research/

The effect of nanosilica sizes in the presence of nonionic TX100 surfactant on CO_2 foam flooding

Suriatie Mat Yusuf [a, c, *], Radzuan Junin [a, b], Mohd Akhmal Muhamad Sidek [a, b], Muhammad A. Manan [a, b], Mohd Fazril Irfan Ahmad Fuad [c], Mohd Zaidi Jaafar [a, b], Effah Yahya [a, c], Nor Roslina Rosli [c]

[a] Department of Petroleum Engineering, School of Chemical and Energy Engineering, Faculty of Engineering, Universiti Teknologi Malaysia, 81310, Johor Bahru, Malaysia
[b] Institute for Oil and Gas, Universiti Teknologi Malaysia, 81310, Johor Bahru, Malaysia
[c] School of Chemical Engineering, College of Engineering, Universiti Teknologi MARA, 40450 Shah Alam, Selangor, Malaysia

ARTICLE INFO

Article history:
Received 11 April 2021
Received in revised form
28 June 2021
Accepted 28 June 2021
Available online 30 June 2021

Keywords:
Nanosilica
Nanoparticle sizes
Adsorption
Nonionic surfactant
TX100 surfactant
Foamability
CO_2 foam stability
CO_2 foam flooding
EOR

ABSTRACT

The aim of this research is to study the effect of hydrophilic silica nanoparticles, sizes as CO_2 foam stabilizer in the presence of nonionic TX100 surfactant. Two nanosilica sizes, 15 and 70 nm, have been examined thoroughly. Physisorption of TX100 on silica nanoparticles (nanosilica) was characterized by adsorption isotherm and surface tension measurement, while CO_2 foams stability was quantified based on their foamability, foam stability, particle partitioning in the foams, and bubble sizes. Results show that direct contact of TX100 with nanosilica does altered the wettability of hydrophilic nanosilica surface, enable them to lengthen CO_2 foams life at certain surfactant and nanoparticles concentrations. For 15 nm nanosilica, CO_2 foam stability shows excellent performance at 0.1 and 0.5 wt% TX100 concentrations. As for 70 nm nanosilica, CO_2 foam demonstrates longer lifetime at much lower TX100 concentration, 0.01 wt%. Without the presence of TX100, CO_2 foams exhibit undesirable lifetime performances for both nanosilica sizes. Nanosilica partitioning in CO_2 foams structures demonstrate consistent relation with contact angle measurement. Estimated bubble sizes shows insignificant effect on CO_2 foams life. With the assists of nanosilica and TX100, enhanced oil recovery via CO_2 foam injection succeeds in increasing oil production by 13–22% of original oil-in-place (OOIP).

1. Introduction

Utilizing particles in stabilizing aqueous foam become preferable in various industrial application as it is solid, dissoluble, and thus offers long term foam life. They behave similar to that of surfactant molecules, except for much stronger attachment (Binks, 2002; Espinoza et al., 2010; Fujii and Murakami, 2008; Horozov, 2008; Hunter et al., 2009b; Karakashev et al., 2011; Kruglyakov et al., 2011). Their ability in adsorbing at gas-water interfaces and consequently stabilizing the foams strongly influenced by particles sizes, shape, concentrations, and surface wettability (Blute et al., 2007; Fan et al., 2004; Yekeen et al., 2018). The mechanism has been studied thoroughly, previously (Horozov and Binks, 2006; Horozov, 2008). Contrary, foam instability happened due to coalescence and disproportionation phenomena (Fujii and Murakami, 2008; Fujii et al., 2006). Since fine particles capable in providing steric barrier at the interface and thin film, and consequently minimizing the abovementioned phenomena, nanoparticles reassure a promising results as foam stabilizer (Fujii and Murakami, 2008; Horozov, 2008).

Silica nanoparticles (SiO_2 NPs) of 20–70 nm range in sizes has been tested alongside anionic surfactant where foam stability increased gradually in the presence of much finer NPs (Tang et al., 1989). Using various surface modifiers, smaller particles seemingly

* Corresponding author. Department of Petroleum Engineering, School of Chemical and Energy Engineering, Faculty of Engineering, Universiti Teknologi Malaysia, 81310, Johor Bahru, Malaysia.
E-mail address: suriatie0539@uitm.edu.my (S.M. Yusuf).

https://doi.org/10.1016/j.ptlrs.2021.06.004

preferable in stabilizing the foams, with or without the presence of surfactants, with respect to particles concentrations (Bayat et al., 2016; Blute et al., 2007, 2009; Fujii et al., 2006; Gonzenbach et al., 2006). Performance of larger particles, approximately 400 nm in sizes, are comparable to that of surfactants stabilizer (Tang et al., 1989). Influenced by dispersions pH, alumina powder of 29–1800 nm sizes, generates finest and stable foams at smallest particles (Gonzenbach et al., 2006). In other studies, instead of highlighting on the adsorption of particles at the interfaces, fine silicas were concluded to form aggregates inside liquid thin film, thus slowing down the drainage, and further stabilized the foam (Carn et al., 2009; Guignot et al., 2010; Hunter et al., 2008b). Oppositely, adverse effect was obtained by 5 nm compared to 150 nm nanosilica, resulting from the surface chemistry (Worthen et al., 2012).

Numerous studies on foams stabilized by SiO_2 NPs have been conducted with the assist of various surfactant as surface modifiers such as alkylpoly(oxyethylene) (Binks et al., 2007), sodium dodecylsulfonate (SDS) (Karakashev et al., 2011; Tang et al., 1989), ethoxylated amine (Zhang et al., 2020), cetyltrimethylammonium bromide (Dong et al., 2010), polyethylene glycol (Worthen et al., 2012), trimethyl(tetradecyl)ammonium bromide (Carn et al., 2009), and many others. From these studies, foam stability showed great improvement as surfactant increases from low to moderate concentration range (Cui et al., 2010; Dong et al., 2010; Hunter et al., 2009b; Liu et al., 2010; Tang et al., 1989). Longer foams life was also being observed as particles concentration increases, even up to 10 wt% (Blute et al., 2007; Carn et al., 2009; Dickinson et al., 2004; Espinoza et al., 2010; Fujii et al., 2006; Kettlewell et al., 2007; Tang et al., 1989). Hunter et al. (2009a) studied the effect of 300 nm octyl grafted silica in the presence of nonionic TX100 surfactant. This combination has improved foam stability within specific TX100 range, low to moderate. All chemicals listed however, only been testes for foam generated with air.

Enhanced oil recovery (EOR) involves the injection of fluid or fluids to displace oil to production well after waterflooding become uneconomical. CO_2 foam flooding are among the processes in impeding gas mobility for control conformance purpose due to porosity and permeability heterogeneities (Bai, 2008). Foam refers to as dispersion of discontinuous gas phase in continuous liquid phase separated by lamellae (Chang and Grigg, 1999). As much as 10–30% of original oil-in- place (OOIP) are being recovered by field implementation of surfactant stabilized CO_2 foams flooding (Xu et al., 2016; Zhang et al., 2014; Zhu et al., 2013). Laboratory studies show that nanoparticles assisted foam process contributed to about 10–40% of OOIP after conventional waterflooding (Li et al., 2016; Sun et al., 2014; Yusuf et al., 2013; Zhao et al., 2021; Zhu et al., 2017). Nanoparticles stabilized CO_2 foam study received wide interest among researchers (Bayat et al., 2016; Emrani et al., 2017; San et al., 2017; Worthen et al., 2012; Zhang et al., 2009; Zhu et al., 2017). Research on the combination of nanosilica – TX100 however, is rarely to be found (Yekeen et al., 2021a; Yusuf et al., 2013). TX100 is preferable for synergetic effect approaches as previous study shows high adsorptivity on negatively oxide surfaces, primarily raw silica particles (Parida et al., 2006; Yekeen et al., 2021a; Yusuf et al., 2013). Furthermore, adsorption of TX100 on hydrophobic nanosilica was previously found to be effective at low to moderate concentrations (Hunter et al., 2008a), making the whole process economically viable. Hence, this study continuing efforts was performed to gather further information on the effect of nanosilica and TX100 in stabilizing CO_2 foams. We used two different particle sizes at various concentrations and extend the study up to their performance in porous media.

2. Materials and methods

2.1. Materials

Amorphous hydrophilic nanosilica of two different sizes were prepared. Nanosilica with size of 15 nm was purchased from MK Impact Corp with 99.5% purity and specific surface area of 650 m^2/g. Meanwhile, 70 nm nanosilica was supplied by Nanoparticles Inc. having 98% purity. Both types of nanosilica appeared as white powder. Nonionic Triton X-100 (TX100) surfactant, of 98% purity and 240 cp viscosity, was purchased from Scharlau Chemei, South Africa. Sodium chloride (NaCl) was purchased from Molekula brand and 100% pure. Paraffin oil was supplied by QRec with density and viscosity of 0.85 g/ml and 28.5 cp, respectively. Carbon dioxide (CO_2) gas was supplied by Mega Mount Industrial Gases Sdn. Bhd. with maximum purity of 96%.

2.2. Methods

2.2.1. Nanosilica-TX100 dispersion preparation

Scanning Electron Microscope (SEM) and energy-dispersive X-ray spectroscopy (EDX) analysis were first being performed on both nanosilica using Hitachi Tabletop SEM equipped with EDX analyzer to detect the elements presence. Brine salinity of 2 wt% NaCl was first being prepared. Surfactant of respective fraction was prepared and added into the brine to give final TX100 solution of 0.01, 0.1, 0.5 and 1 wt%, and continuously stirred until homogeneous solution was obtained. Nanosilica concentrations of 0.1, 0.5, 1, 5 and 7 wt% was then being dispersed in TX100 solution using magnetic stirrer at room temperature. Nanosilica-TX100 dispersions were continuously stirred for 12 h to achieve adsorption equilibrium (Dong et al., 2010; Zhang et al., 2008). Phase behavior of the dispersions were consistently observed.

2.2.2. Adsorption of TX-100 on nanosilica

TX100 adsorption on nanosilica surface was estimated by UV depletion method using Buck Scientific 105 UV-Vis Spectrophotometer. Dispersions were centrifuged at 15000 rpm for 20 min and the supernatants were analyzed thoroughly. TX100 aqueous solution peak was found at 290 nm. Final concentration of remaining TX100 after adsorption period was calculated from absorbance plot obtained (Binks et al., 2006; Hunter et al., 2009b; Ledakowicz et al., 2005).

2.2.3. Nanosilica-TX100 dispersion viscosity

Anton-Paar rheometer was used to measure nanosilica-TX100 dispersion viscosity. The measurement was performed at ambient condition. All measurements were run 3 times for precision reading.

2.2.4. Surface tension of Nanosilica-TX100 dispersions

Conventional method in determining surface tension of dispersion was performed using Kruss Tensiometer apparatus through du Nouy Ring method with proper correction factor (ASTM-D971-99a, 2004; Zuidema and Waters, 1941). Surface tension increment in equilibrated nanosilica-TX100 dispersions also confirmed the loss of TX100 monomers to nanosilica surface due to adsorption process.

2.2.5. Foamability and foam stability

Modified laboratory blender with a stream of CO_2 gases was used in generating the foams. Dispersions of 50 ml volume were blended at 14,000 rpm for 2 min while simultaneously being

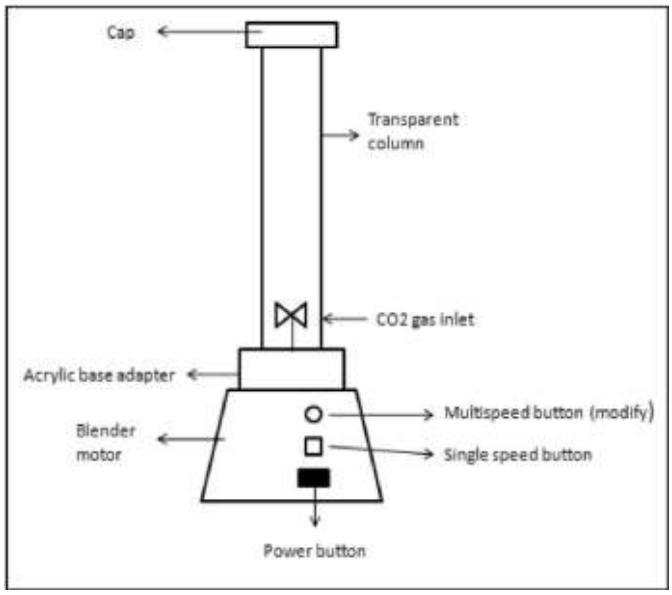

Fig. 1. Modified CO_2 foam generator (Dellinger et al., 1984; Yusuf et al., 2013).

supplied with CO_2 (Alkan et al., 1991; ASTM D 3519-88, 2007; Liu et al., 2009; Zhang et al., 2008). Immediately after stopping the blender, foam height in the graduated blender column was determined and recorded. Height of foam was continuously observed and recorded every 5 min time interval. Normalized foam height was computed as a function of time (Andrianov et al., 2012; Yusuf et al., 2013; Zhang et al., 2008). Fig. 1 illustrates the modified CO_2 foam generator adapted from the previous studies where the height-to-diameter ratio is increased for precision measurement (ASTM D 3519-88, 2007; Dellinger et al., 1984; Yusuf et al., 2013). The diameter and height of the transparent acrylic column are 6.4 cm and 39 cm, respectively.

2.2.6. Bubble sizes of foam

Immediately after foam generation, adequate amount of the bubbles was acquired and observed under Leica EZ4 HD Stereo Microscope. The images were captured accordingly for bubble sizes estimation.

2.2.7. Nanosilica partitioning in generated foams

Following foam generation, it was then allowed to settle for 30 min. Syringe was then being used to collect liquid drained underneath foam bulk. The collected liquid was dried at 105 °C. Fraction of nanosilica attached on foams were estimated by differencing the particles weight during dispersion preparation and after 30 min it was being drained (Cui et al., 2010; Zhang et al., 2008).

2.2.8. Estimation of contact angle changes with TX100 concentration

Microslides were used in mimicking the characteristic of nanosilica surfaces as both silica and TX100 concentrations were being manipulated. Glass microslides were immersed in various nanosilica-TX100 dispersions samples for 24 h (Hunter et al., 2009b). Contact angle of droplet deionized water on planar dried microslides was then being observed and determined using Kruss contact angle meter.

2.2.9. EOR by CO_2 foams stabilized by Nanosilica-TX100 dispersions

Tertiary recovery was carried out by performing sandpack flooding. Transparent sandpack column of 3.9 cm diameter x 33 cm length was packed and compacted with sand grains of less than 350 μm in sizes. Fig. 2 shows the schematic diagram of the experiment setup. Sandpack column was set in vertical orientation, fitted with pressure gauge at the inlet and outlet. Sandpack properties; permeability (k), pore volume (PV), porosity (Ø), initial water saturation (Sw_i) and residual oil saturation (So_r) was estimated thoroughly. Waterflooding was performed at 0.5 ml/min until uneconomical amount of oil was measured. After waterflooding was terminated, CO_2 foam flooding was conducted immediately. Gas and aqueous dispersion were co-injected at CO_2 to nanosilica-TX100 dispersion ratio of 30:1 for in-situ foam generation (Andrianov et al., 2012; Haugen et al., 2012). Volume of effluents were collected and recorded. All the experiments were conducted at ambient condition.

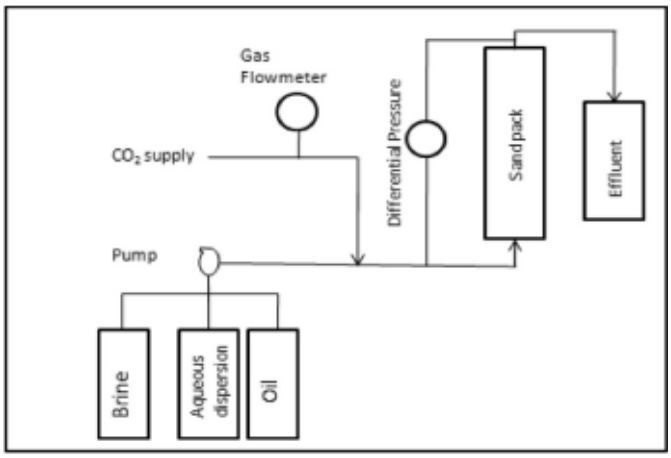

Fig. 2. CO_2 foam flooding experimental setup.

3. Results and discussion

3.1. Nanosilica-TX100 dispersions phase behavior

SEM analysis (Fig. 3, Fig. 4) shows that both nanosilicas are homogeneously spherical in shape and sizes. The actual sizes are slightly bigger than provided by the supplier, 15 nm sizes are ranged 15–40 nm, while 70 nm varies within 60–90 nm. Both

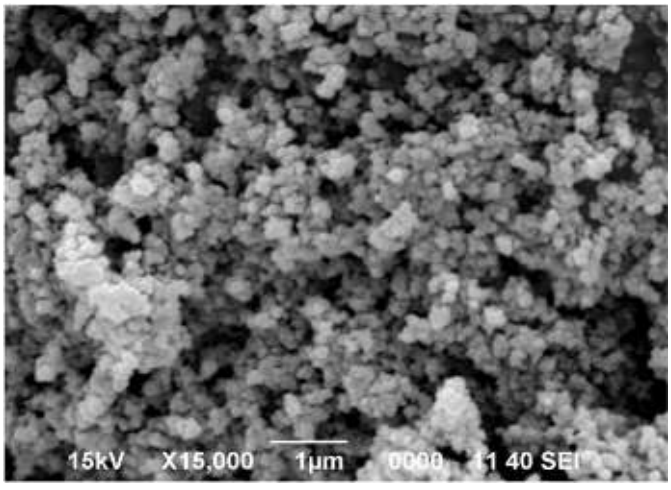

Fig. 3. SEM image of 15 nm nanosilica.

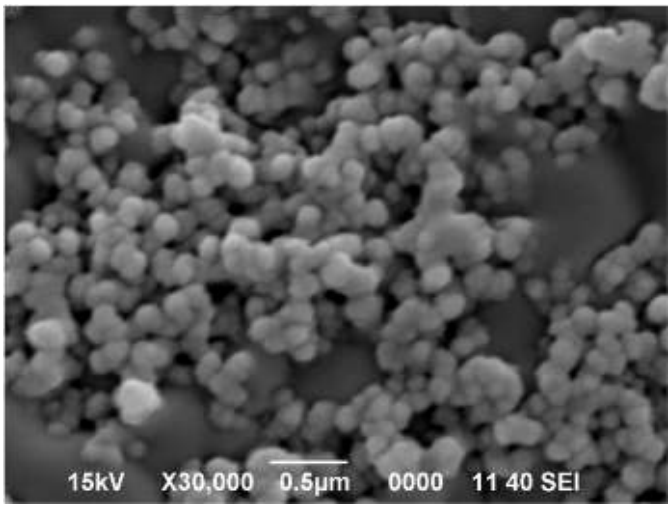

Fig. 4. SEM image of 70 nm nanosilica.

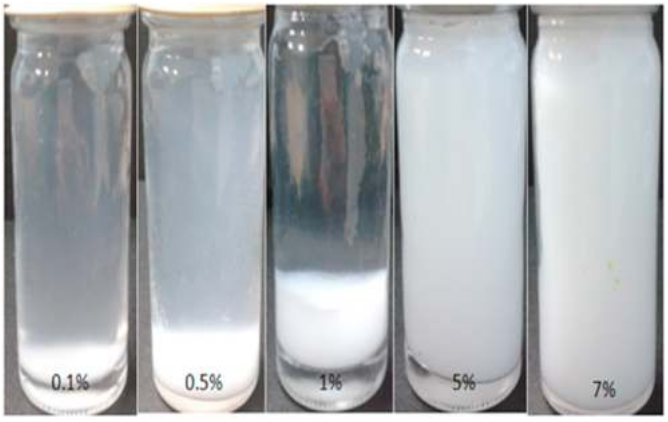

Fig. 5. Phase behavior of 15 nm nanosilica and 0.1 wt% TX100 dispersions at various nanosilica fraction.

particles hereafter will be denoted as 15 and 70 nm sizes, respectively. Cloudy or hazy dispersion was considered stable as the particles repulsion occurs, distributed uniformly in bulk liquid system (Dong et al., 2010). The hazier the dispersion, more stable it is. Contrary, unstable dispersion was classified as particles settled at the bottom of bulk dispersion, indicating particles flocculation (Zhang et al., 2008). Fig. 5 and Fig. 6 illustrate phase behavior of nanosilica-TX100 dispersions at 0.1 wt% surfactant for 15 nm, and 0.5 wt% surfactant for 70 nm nanosilica, respectively. At lower particles concentrations, 0.1 and 0.5 wt%, cloudy dispersions were observed for both nanosilica sizes, indicating stable dispersions. At 1 and 5 wt% nanosilica, dispersions show total phase separations with particles totally settled at the bottom of the bottles. Further increases to 7 wt%, particles occupied the whole liquid bulk volume, with gel-like behavior. It should be noted that for 5 and 7 wt% 15 nm nanosilica, heavily saturated gel-like colloidal system was generated instead of dispersions, for all TX100 concentrations. This gel-like formation was speculated due to the increment of particles sizes due to the formation of TX100 monolayer adsorbed on particles surfaces (Dong et al., 2010; Giordano-Palmino et al., 1994; Zhang et al., 2008). So instead, we eliminated the formulations at those combinations and tested the relatable parameters (contact angle, foam stability, particles partitioning, and bubble sizes) at much lower nanosilica concentration, 2 wt% nanosilica. Other formulation of silica-TX100 dispersions behavior were summarized in Tables 1 and 2 for 15 nm and 70 nm sizes, respectively. For EOR purpose, stable dispersion is main parameter to be considered for proper foam generation and CO_2 dissolution in the dispersion.

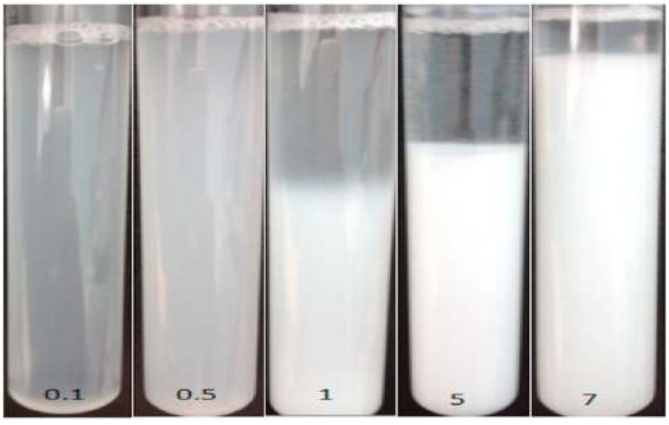

Fig. 6. Phase behavior of 70 nm nanosilica and 0.5 wt% TX100 dispersions at various nanosilica fraction.

3.2. Adsorption of TX100 on nanosilica

Adsorption isotherm of TX100 on nanosilica surface was analyzed thoroughly. Tables 3 and 4 tabulate the adsorption of TX100 on 15 nm and 70 nm nanosilica, respectively, and their classifications. UV-depletion method was used to estimate the adsorption. Absorption peak of TX100 was found at 290 nm wavelength, slightly higher than previous studies (Ledakowicz et al., 2005; Zeng and Osseo-Asare, 2004). By nature, surfaces of hydrophilic silica are abundant with silanol groups (Ivanova et al., 1995; Parida et al., 2006; Zhuravlev, 2000), and was confirmed by EDX analysis (Fig. 7 and Fig. 8). Significant peak observed indicating the surface is highly saturated with silicon (Si) and oxide (O) elements. Silanol groups provide free surfaces for TX100 adsorption in bulk dispersion through physisorption. TX100 solute may uptakes nanosilica surface via van der Waals attractions without any chemical reaction (Levitz et al., 1984; Levitz and Van Damme, 1986). Adsorption of TX100 on hydrophilic silica surface occurs as the molecules aggregate in orderly manners, similar to that of regular micelles (Levitz et al., 1984; Levitz and Van Damme, 1986).

From Tables 3 and 4, TX100 loss to vacant silica surface was verified as the percentage of adsorbed solute is high up to more than 90% of initial surfactant concentration. Adsorption vs equilibrium concentration plot was further used Langmuir adsorption isotherm classification (Giles et al., 1974a, 1974b). The L-curve isotherm indicates nanosilica surface changes partially hydrophobic in steadily manners. C-curve isotherm suggests the available surface for adsorption is proportional to the amount of solute being

Table 1
Phase behavior of 15 nm nanosilica – TX100 formulations.

TX100, wt% (→) / Nanosilica, wt% (↓)	0.01	0.1	0.5	1
0.1	Sediment	Cloudy	Cloudy	Heavily cloudy
0.5	Sediment	Cloudy	Cloudy	Heavily cloudy
1	Sediment	Sediment	Cloudy	Heavily cloudy
5	Gel	Sediment	Gel	Gel
7	Gel	Gel	Gel	Gel

Table 2
Phase behaviour of 70 nm nanosilica – TX100 formulations.

TX100, wt% (→) / Nanosilica, wt% (↓)	0.01	0.1	0.5	1
0.1	Slightly cloudy with sediment	Slightly cloudy with sediment	Heavily cloudy	Heavily cloudy
0.5	Sediment	Slightly cloudy with sediment	Heavily cloudy	Heavily cloudy
1	Cloudy and sediment	Sediment	Cloudy and sediment	Heavily cloudy
5	Cloudy	Sediment	Sediment	Sediment
7	Sediment	Gel	Sediment	Sediment

Table 3
Adsorption of TX100 on 15 nm nanosilica and isotherm classification.

Nanosilica conc, %	0.1		0.5		1		5		7	
Initial TX100 conc, %	Equil. conc, %	% Adsorption	Equil. conc, %	% Adsorption	Equil. conc, %	% Adsorption	Equil. conc, %	% Adsorption	Equil. conc, %	% Adsorption
0.01	0.004	56.400	0.004	60.000	0.004	63.500	0.004	64.308	0.004	64.792
0.1	0.040	60.000	0.007	92.900	0.005	95.000	0.005	95.200	0.004	95.640
0.5	0.295	41.000	0.238	52.350	0.076	84.800	0.007	98.528	0.007	98.640
1	0.644	35.636	0.597	40.255	0.516	48.436	0.012	98.760	0.010	99.040
Isotherm class	**L**		**L**		**L**		**C**		**C**	

Table 4
Adsorption of TX100 on 70 nm nanosilica and isotherm classification.

Nanosilica conc, %	0.1		0.5		1		5		7	
Initial TX100 conc, %	Equil. conc, %	% Adsorption	Equil. conc, %	% Adsorption	Equil. conc, %	% Adsorption	Equil. conc, %	% Adsorption	Equil. conc, %	% Adsorption
0.01	0.0052	47.520	0.0070	29.600	0.0044	55.731	0.0079	21.000	0.0059	41.000
0.1	0.0283	71.700	0.0128	87.200	0.0253	74.700	0.0095	90.540	0.0158	84.200
0.5	0.3225	35.500	0.2675	46.500	0.0980	80.400	0.0205	95.900	0.0214	95.720
1	0.4075	59.250	0.3550	64.500	0.4350	56.500	0.0300	97.000	0.0235	97.648
Isotherm class	**L**		**L**		**L**		**C**		**S**	

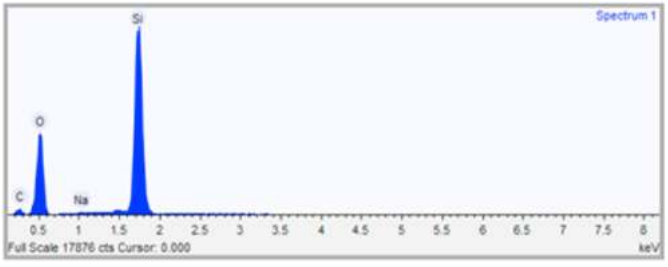

Fig. 7. EDX analysis for 15 nm nanosilica.

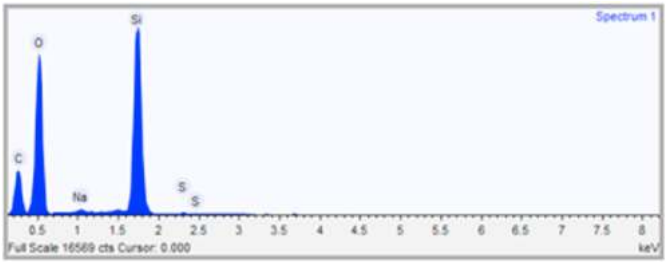

Fig. 8. EDX analysis for 70 nm nanosilica.

adsorbed. Tables 3 and 4 confirmed this statement as the percent of TX100 adsorbed is high enough at high nanosilica concentrations. S-shape signifies the clustered or clumped molecules adsorbed on solid surface. Particles may grow bigger due to particles agglomerated, as being observed in dispersion behaviour. Rapid changes to

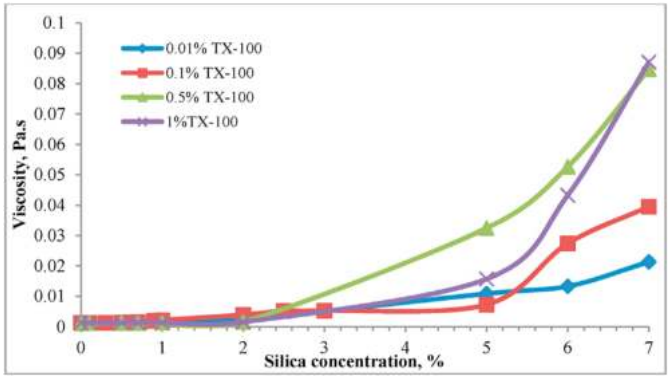

Fig. 9. 15 nm nanosilica – TX100 dispersions viscosity.

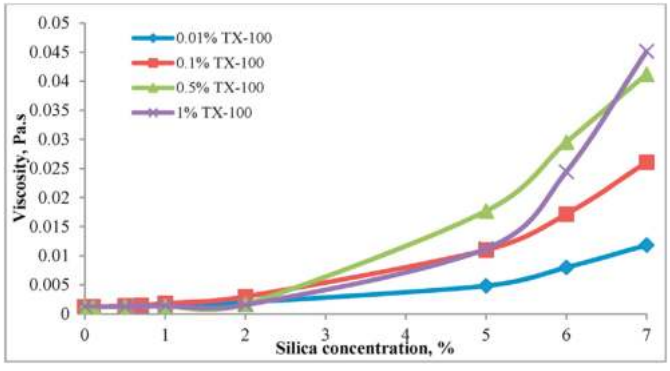

Fig. 10. 70 nm nanosilica – TX100 dispersions viscosity.

hydrophobic behaviour was expected for this isotherm type (Giles et al., 1974b). From adsorption study, TX100 adsorbed on 15 nm is higher than 70 nm, proves more vacant surface area is available for smaller particles.

3.3. Viscosity of Nanosilica-TX100 dispersion

Viscosity of dispersions were plotted in Fig. 9 and Fig. 10 for 15 nm and 70 nm nanosilica, respectively. For both particle sizes, it is definite that viscosity increases steadily with nanosilica concentrations. Smaller particle shows twice as high the viscosity value, indicating higher number of particles per unit volume at the same concentration compared to 70 nm nanosilica. An intriguing pattern was observed at 1 wt% TX100. For both nanosilica sizes at this surfactant concentration, viscosity is much lower compared to that of at 0.5 wt% TX100. The rationale behind this probably lies on the high adsorption of TX100 on nanosilica surface which consequently increase particles flocculation and sedimentation. In foam formations, dispersion viscosity plays a crucial factor as it reflects the liquid drainage behavior and further increase foam stability. Aside from attachment at gas-liquid interface, excess particles volume in aqueous bulk or typically highly hydrophilic particles, may occupy and form aggregates in foam liquid film, slowing down the drainage, thus, improve foam stability (Adkins et al., 2007; Horozov, 2008).

3.4. Surface tension of dispersion

Using Kruss tensiometer with platinum-iridium ring, surface tension reduction of nanosilica-TX100 dispersions were measured and analyzed. Fig. 11 and Fig. 12 present the outcome of this measurement at 0.1 and 5 wt% nanosilica, respectively. Surface tension reduction for 0.5, 1, and 7 wt% nanosilica, were also being plotted and analyzed. Tables 5 and 6 tabulate surface tensions at equilibrium TX100 concentrations. Significant trend was observed from all nanosilica-TX100 combinations, smaller silica possesses lower surface tension reduction compared to 70 nm nanosilica. Significant increment in surface tension with nanosilica fraction was clearly observed. This implies the loss of TX100 monomers to particle surface due to adsorption process. At each nanosilica fraction, reduction shows quite similar pattern, suggesting the same mechanism involves. For 15 nm nanosilica, the trend is quite identical to that of being studied previously (Binks et al., 2006; Hunter et al., 2009b; Somasundaran et al., 1991). Abrupt increased in surface tension at of 70 nm nanosilica demonstrates the high micelles formation on nanosilica surface. Remaining TX100 molecules in bulk solutions reduced as a result of adsorption process and

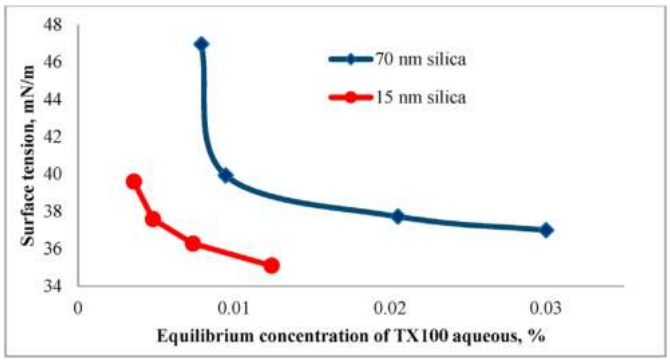

Fig. 12. Surface tension of dispersion at 5 wt% nanosilica.

Table 5
Surface tension (mN/m) of pre-equalized 15 nm nanosilica-TX100 dispersion.

Nanosilica conc, % (→) / Initial TX100 conc, % (↓)	0	0.1	0.5	1	5	7
0.01	31.956	34.847	35.064	36.848	39.598	43.518
0.1	31.471	31.036	32.163	35.961	37.583	43.494
0.5	30.398	30.942	31.816	32.252	36.279	38.082
1	31.162	31.772	32.258	32.243	35.091	37.321

Table 6
Surface tension (mN/m) of pre-equalized 70 nm nanosilica-TX100 dispersion.

Nanosilica conc, % (→) / Initial TX100 conc, % (↓)	0	0.1	0.5	1	5	7
0.01	31.953	35.874	37.798	39.363	46.952	49.317
0.1	31.468	32.142	34.115	36.736	39.932	41.498
0.5	30.395	32.439	32.585	32.847	37.725	40.179
1	31.159	34.557	33.748	35.019	36.988	36.436

was verified by surface tension increment. It is highly suspected that at higher nanosilica concentrations (5 and 7 wt%), particles agglomeration and flocculation occur, hindering TX100 solute from filling up silica surfaces. Thus, going from 0.01 to 1 wt% TX100 for both nanosilica sizes, appreciable surface tension reduction was clearly observed, suggested the high remaining unadsorbed TX100 solutes in bulk solutions. From Figs. 11 and 12, it is strongly convinced that no secondary interaction (chemical reaction) takes place other than surface tension reduction due to physisorption phenomena (Levitz and Van Damme, 1986; Levitz et al., 1984). Silica presence in aqueous system was known to have no effect on surface

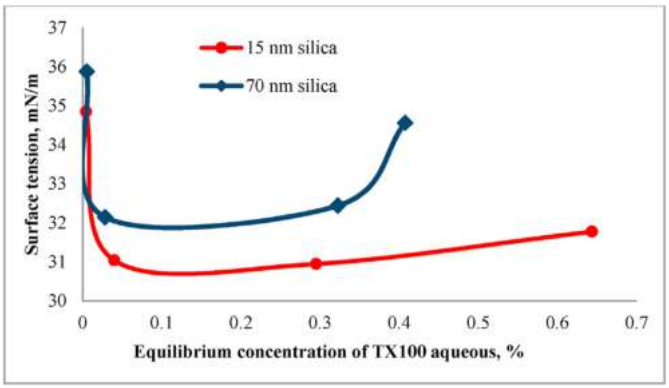

Fig. 11. Surface tension of dispersion at 0.1 wt% nanosilica.

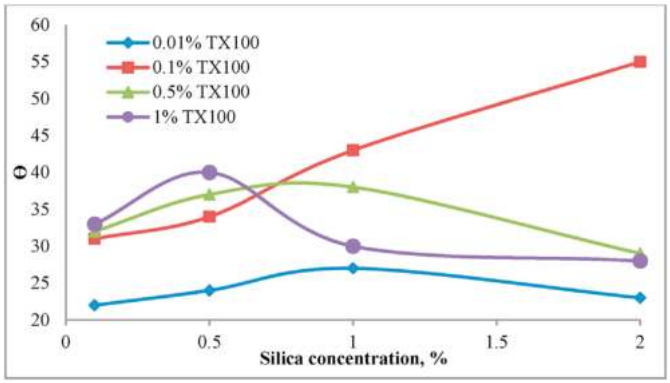

Fig. 13. Estimated contact angle of 15 nm nanosilica-TX100.

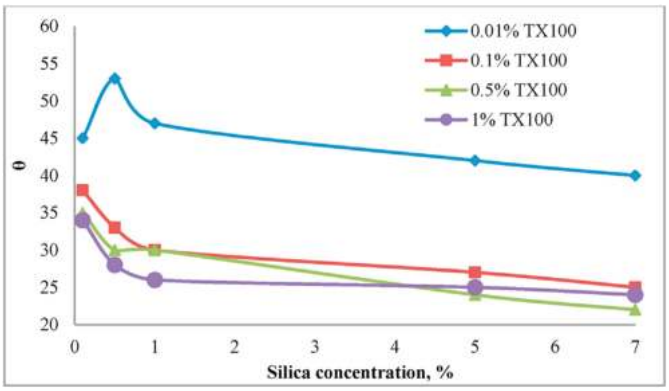

Fig. 14. Estimated contact angle of 70 nm nanosilica-TX100.

tension reduction (Okubo, 1995). They also does not facilitates in bringing surfactant monomers to gas-liquid interfaces for the same purpose (Ravera et al., 2006). Adsorption and surface tension analysis both evidently shows that hydrophilic silica particles used in this study does turn partially hydrophobic to a certain extend.

3.5. Contact angle measurement

Fig. 13 and Fig. 14 illustrate the estimated contact angle (θ) of 15 and 70 nm nanosilica-TX100 combinations as a function of nanosilica concentrations. Both nanosilicas possess contact angle in a range of approximately 22–55°. Initially, the contact angle without any additional TX100 was measured where the droplet spread evenly on microslide, indicating totally hydrophilic behavior, as being obtained from manufacturer. In the addition of TX100, particles do turn partially hydrophobic to certain extent, rendering them favorably possible to be attached on CO_2 – water interfaces. These nanosilicas are presumed to reside more on liquid film region in stabilizing CO_2 foams (Binks and Horozov, 2005; Binks, 2002; Binks et al., 2007; Horozov, 2008; Horozov and Binks, 2006). For both particles, at low TX100 concentrations (0.01 and 0.1 wt%), contact angle for 70 nm nanosilica is much higher compared to that of 15 nm, which support the result of adsorption and surface tension measurements. At higher TX100, insignificant different in contact angle was obtained. Contact angle for smaller nanosilica shows an alternate trend except for 0.1 wt% TX100, where increasing hydrophobicity was observed. For the rest, contact angle increased and then decreased gradually indicating the transition of surface wettability, from low to marginally high, and then turned back to low hydrophobic condition. We strongly believe this double inversion behavior highly affecting CO_2 foam stability as being discussed in next section. For 70 nm nanosilica, lowest TX100 gives highest hydrophobic conditions. Increasing surfactant concentrations displays significant contact angle reduction with respect to nanosilica fractions.

3.6. Foam stability and particle partitioning

Static experiment for screening the formulation for CO_2 foams stabilizers was viewed as practical and sufficiently useful in determining the foaming properties, particularly in such cases where numerous combinations were to be tested (Borchardt et al., 1985). Foam stability, quantified as normalized foam height, are presented in Fig. 15 and Fig. 16. CO_2 foams were generated at 96% quality. Low foamability was observed in foam generated from liquid suspension compared to TX100 solution alone. Similar outcomes were previously observed by several researchers (Binks and Horozov, 2005; Dickinson et al., 2004; Dong et al., 2010; Vijayaraghavan et al., 2009; Zhang et al., 2008). Should be noted that, for both particles, CO_2 is hardly to diffuse as the suspensions are greater than 2 wt%.

For lowest TX100 concentration (Fig. 15a), foam generated are at least 30% more than TX100 solution alone. Abrupt foam heights were recorded, indicating rapid liquid drained from foam structures. Insignificant effect on foam stability was observed as nanosilica fraction increased. Increasing TX100 (Fig. 15b–d), gradual foam height reductions were observed. The trend corresponds to that of particles attach in foam structure (Fig. 17). Foams tend to collapse faster at the first few minutes and then remain stable with

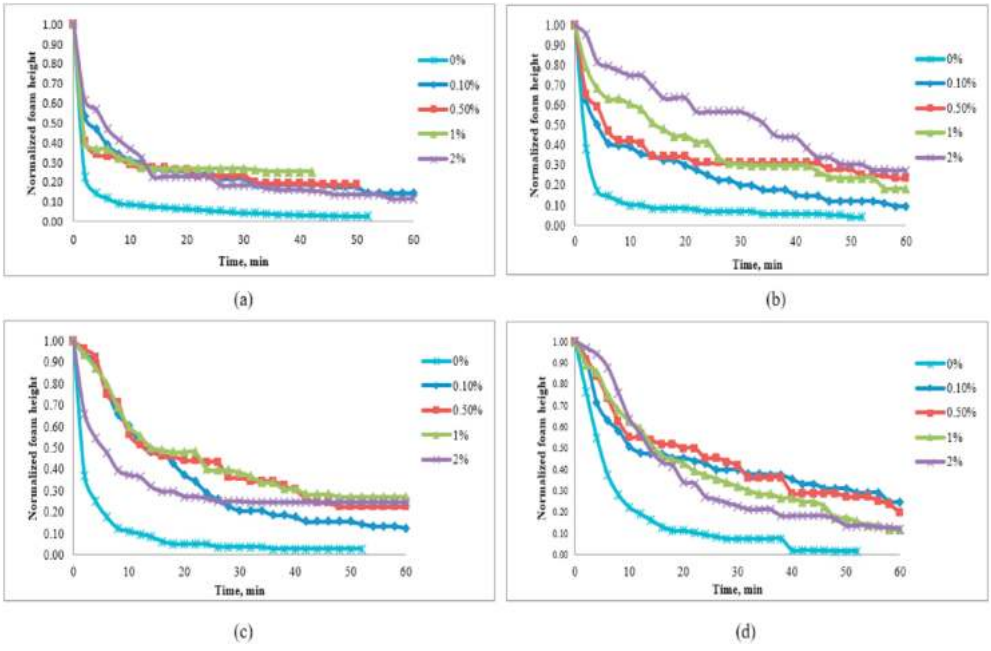

Fig. 15. Normalized foam height of 15 nm nanosilica at (a) 0.01, (b) 0.1, (c) 0.5 and, (d) 1 wt% TX100.

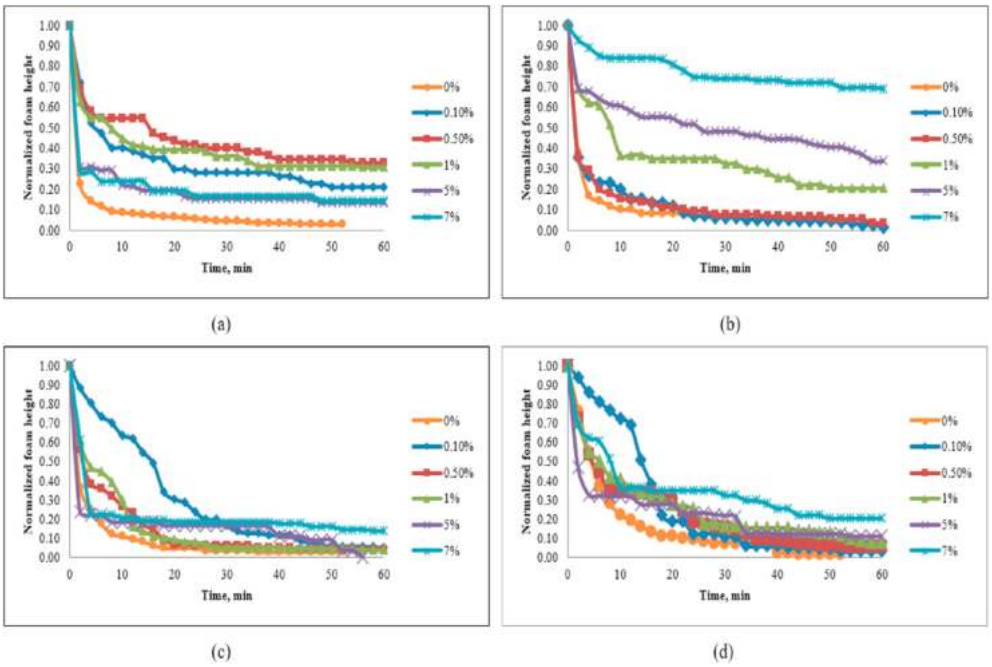

Fig. 16. Normalized foam height of 70 nm nanosilica at (a) 0.01, (b) 0.1, (c) 0.5 and, (d) 1 wt% TX100.

time. Synergetic effect of nanosilica-TX100 were convincedly turned nanosilica partially hydrophobic, attached at CO_2-water interfaces, and consequently stabilized the foams. Increased nanosilica concentration (2 wt%) however, shows insignificant advantages on foam life. Lower to intermediate nanosilica concentrations gives favorable conditions for foam stability. It is notably found that foam structure just above bulk liquid dispersions remained to about 20–40% of initial volume for a long time (several hours and even days). The bubbles were observed to be smaller with much finer textures. Previously, at intermediate to high surfactant concentrations, foam height reduce and results in longer foam life (Zhang et al., 2008). Dense film around the bubbles efficiently hindered coalescence and disproportionation. The aggregated particles consequently reduced liquid drainage.

CO_2 foam generated by 70 nm nanosilica – TX100 dispersions (Fig. 16) shows excellent stability at lower surfactant concentration, from lower to higher particles fractions. This result is consistent with particles partitioning trend (Fig. 18). Insignificant trend was observed in 0.5 and 1 wt% TX100. Foam decayed behavior almost similar to that of TX100 solution only. Nonetheless, congested particles in liquid films are presumed have impeded liquid drainage and further stabilized the foams at higher nanosilica concentrations (Fig. 22B and Fig. 23B). Overall, both nanosilicas (15 and 70 nm) gave a contra results on foam stability; smaller one favors at intermediate TX100 concentration, while the larger particles are compatible at lower TX100 concentration.

3.7. Foam bubble sizes

CO_2 foams generated without the presence of nanosilica were visualized and presented in Fig. 19 with larger and coarse bubbles were observed. The bubbles images were difficult to capture as they tend to collapse immediately after the formations, consistent with foam life in Figs. 15 and 16 (no nanosilica).

From visualization procedure, distinctive results were obtained. Mean bubble sizes reduced with the increased of nanosilica concentrations. For 15 nm nanosilica – 0.01 wt% TX100 (Fig. 20A), insignificant bubble sizes increased with nanosilica concentrations, with the bubbles are close to one another. Dense liquid film with smaller bubbles were observed at 0.1 wt% TX100 (Fig. 21A). Increasing TX100 concentrations to 0.5 (Fig. 22A) and 1 wt% (Fig. 23A) generates much finer bubbles. However, at these TX100

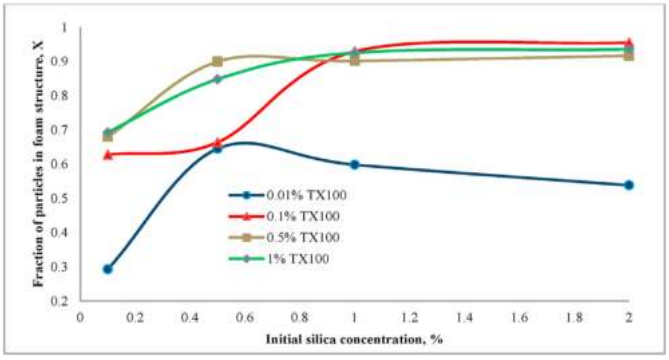

Fig. 17. Estimated fraction of 15 nm nanosilica present in CO_2 foam structure at 30 min.

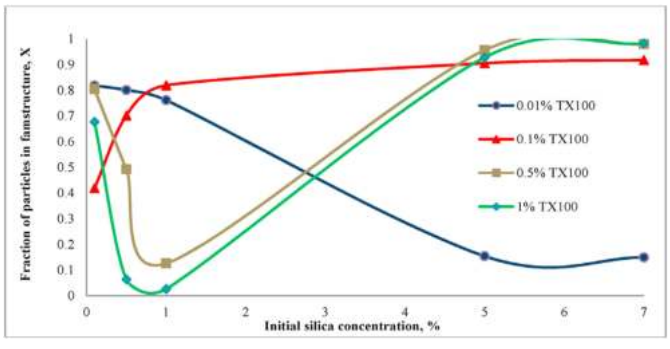

Fig. 18. Estimated fraction of 70 nm nanosilica present in CO_2 foam structure at 30 min.

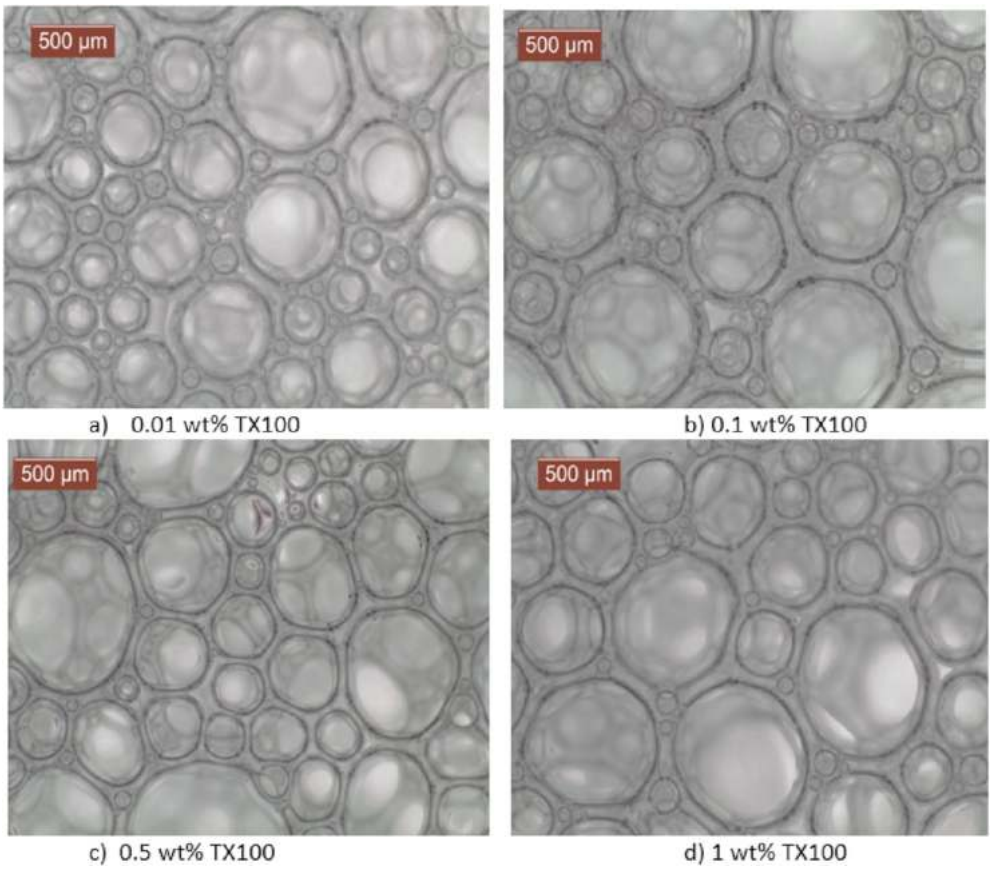

Fig. 19. CO_2 foams generated without the presence of nanoslica. The fractions of TX100 surfactant are labeled accordingly.

concentrations (0.5 and 1 wt%) the presence of 0.1, 0.5, 1 and 2 wt% nanosilica results in liquid film between the bubbles to be much closer, inducing rate of coalescence, further destabilized the foams (Kruglyakov et al., 2008). Less numbers of bubbles can be seen at 5 and 7 wt% nanosilica, indicating the difficulty of CO_2 to diffuse in the gel-like colloidal system to generate the foams.

Figs. 20B, 21B, 22B and 23B show that 70 nm nanosilica generates smaller bubbles for all TX100 concentrations tested. Uniform bubble size distributions were observed at lower to intermediate nanosilica concentrations at 0.1, 0.5 and 1 wt% TX100. At higher nanosilica fractions (5 and 7 wt%) liquid films were occupied with concentrated nanosilica, with less bubbles number were captured. This behavior demonstrates poor foam quality generated as it is getting harder for CO_2 to be diffused in bulk liquid dispersion at higher nanosilica concentrations (Gonzenbach et al., 2006). Figs. 20 to 23 display the images of bubbles captured at respective nanosilica-TX100 combinations. Contrary, from Figs. 17 and 18 where high fractions were estimated and expected to remain intact in CO_2 foam structure at higher nanosilica concentration, it was observed that the concentrated and saturated cake-like layer just above the suspension solutions are hardly to consist of bubbles rather the particles are coagulated and aggregated. Bubble sizes measured shows indirect relations with foam life. Increased in suspension viscosity results in finer bubbles being generated due to the adsorption of amphiphilic species on particle surfaces (Gonzenbach et al., 2006).

3.8. CO_2 foam flooding enhanced oil recovery

Standard procedures in determining porous media properties were conducted. Sandpacks were position vertically to minimize gravity segregation. Porosity, Ø, was determined and kept in between 38 and 41% with permeability, k, ranging from 33.6 to 39.7 Darcy. Prior to CO_2 foam flooding, waterflooding was conducted until the amount of oil obtained is uneconomical enough to be produced. Brine was continuously injected at 0.5 ml/min which is equivalent to 2.46 ft/day velocity. Eight displacement experiments were conducted using several nanosilica-TX100 combinations tested earlier, with promising criteria for EOR applications (dispersion viscosity, foam stability, particles partitioning, contact angle, and bubble sizes). Foams were generated in-situ by co-injecting CO_2 gases and nanosilica-TX100 dispersion. Throughout the procedures, oil recovered, and differential pressure were recorded thoroughly.

3.8.1. TX100 only solution

A base case of TX100 only CO_2 foams flooding was performed at 1 wt% concentration is presented in Fig. 24, with incremental oil recovery recorded is 6.96% of OOIP. Oil started to produce much later than expected, around 2 PV of total foam injection. Sudden peaked up in pressure indicates initial foams generation and build up in the pores. Abrupt reduction and continuous with almost constant pressure imply poor foams quality being produced and possibility CO_2 preferential flow in porous media. Insignificant CO_2 foams blocking effect was strongly presumed throughout the process (Apaydin et al., 1999; Haugen et al., 2012).

3.8.2. 0.1 wt% 15 nm nanosilica – 0.1 wt% TX100

First combination tested was 0.1 wt% 15 nm nanosilica and 0.1 wt% TX100 (Fig. 25). Oil recovery from tertiary recovery reached

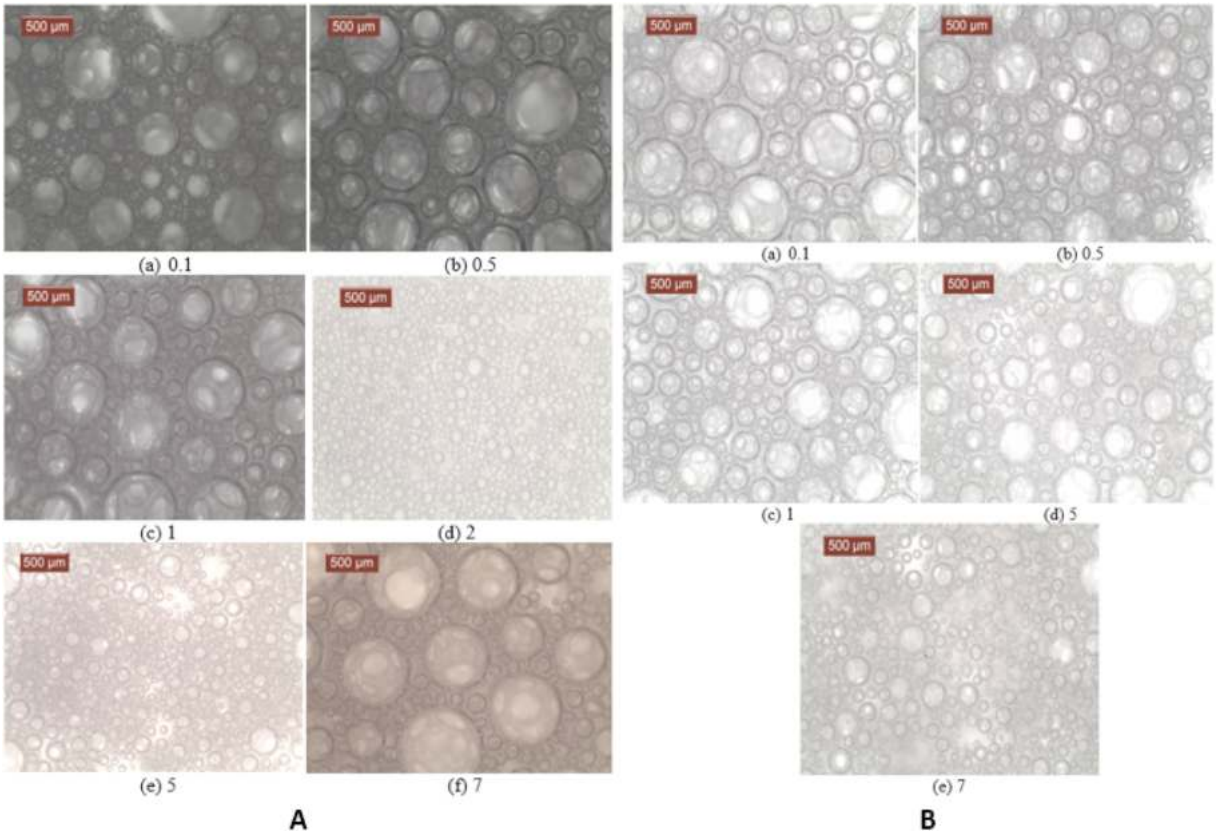

Fig. 20. CO_2 foams generated by 0.01 wt% TX100 with the presence of (A) 15 nm and (B) 70 nm nanosilica.

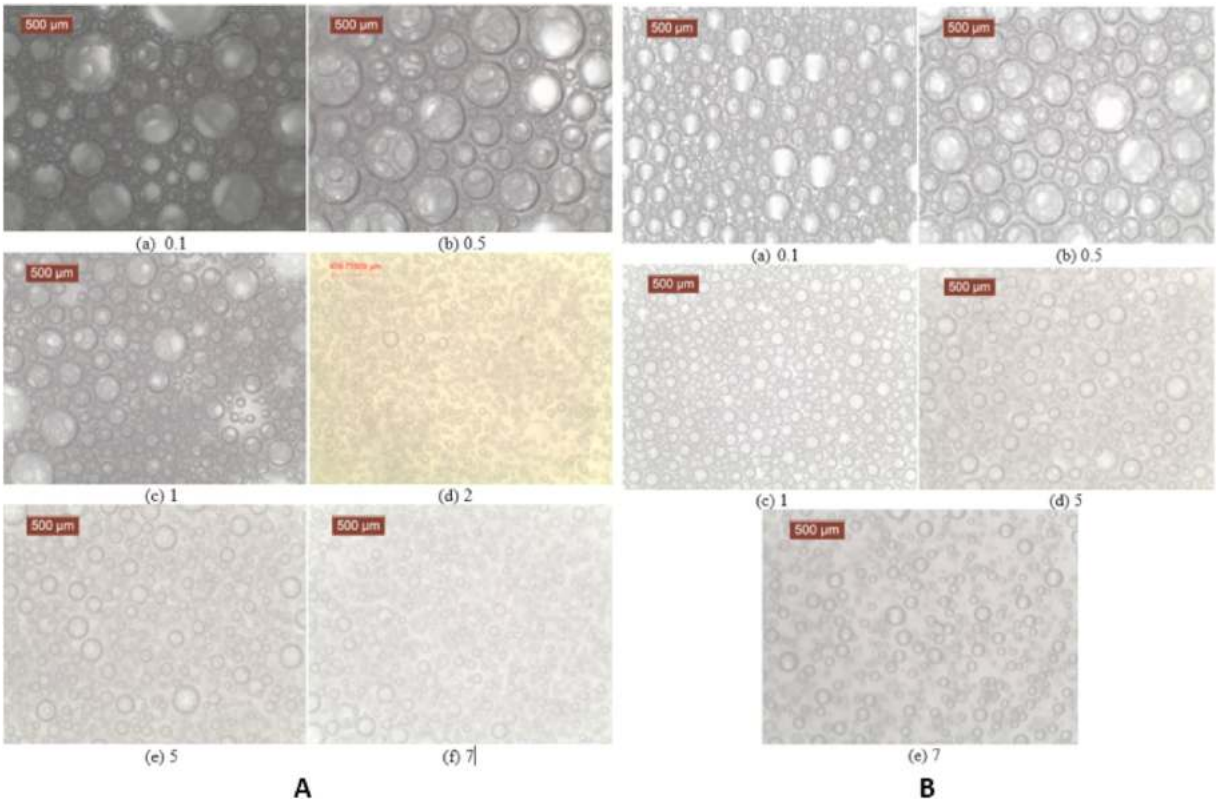

Fig. 21. CO_2 foams generated by 0.1 wt% TX100 with the presence of (A) 15 nm and (B) 70 nm nanosilica.

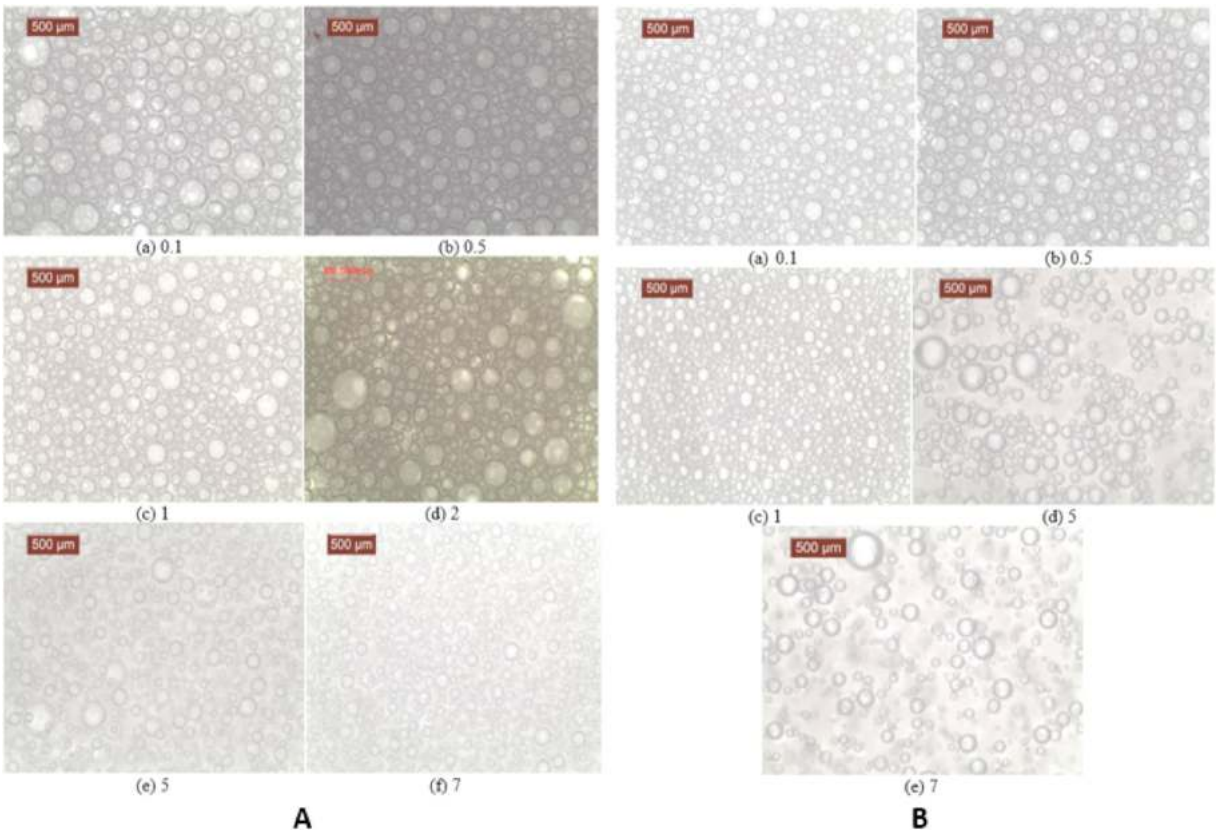

Fig. 22. CO_2 foams generated by 0.5 wt% TX100 with the presence of (A) 15 nm and (B) 70 nm nanosilica.

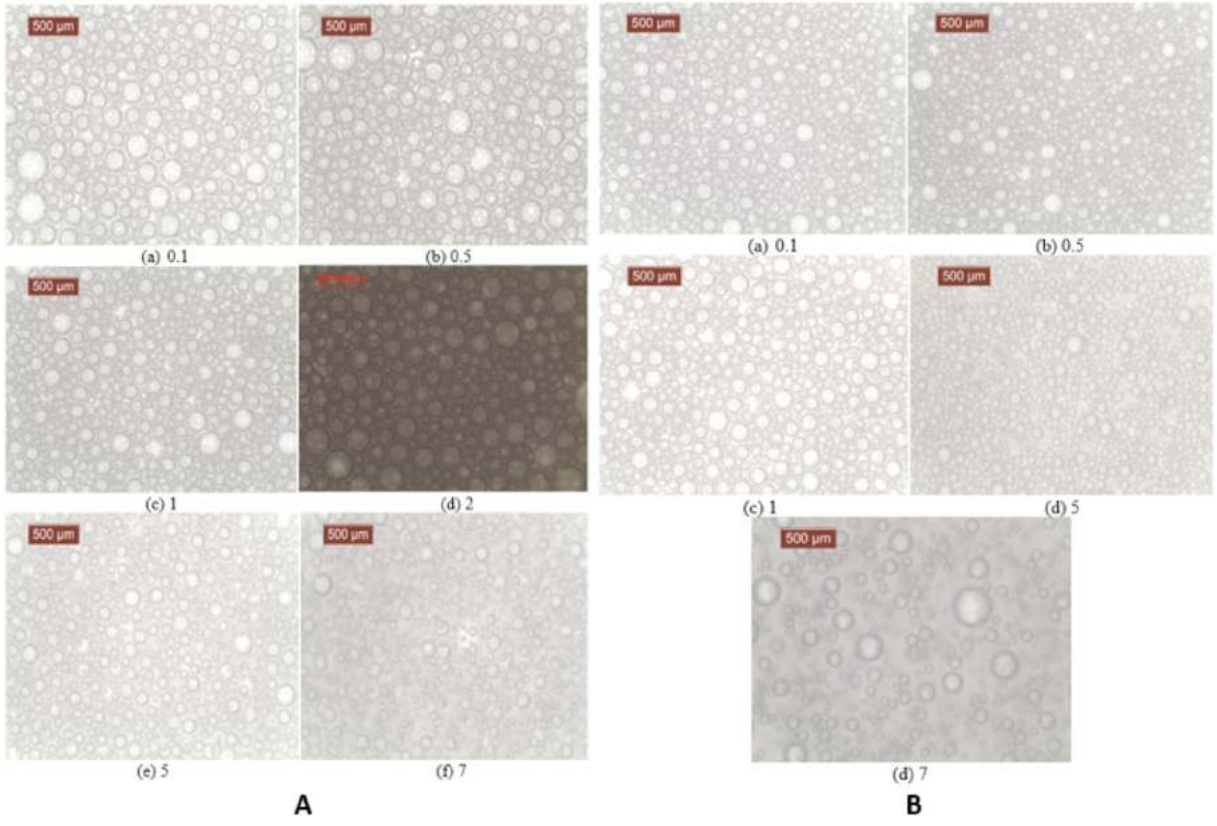

Fig. 23. CO_2 foams generated by 1 wt% TX100 with the presence of (A) 15 nm and (B) 70 nm nanosilica.

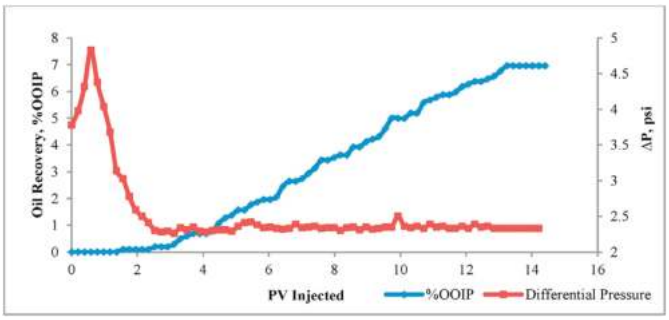

Fig. 24. CO_2 foam flooding using 1 wt% TX100.

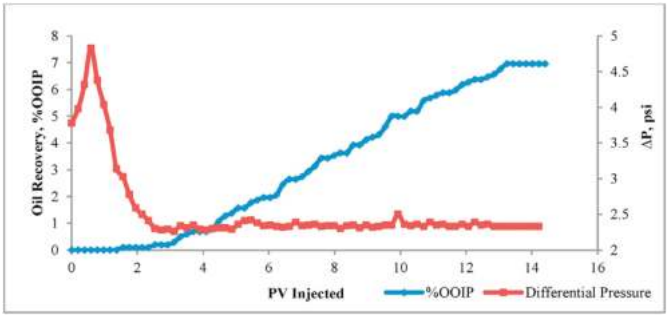

Fig. 25. CO_2 foam flooding using 0.1 wt% 15 nm nanosilica – 0.1 wt% TX100.

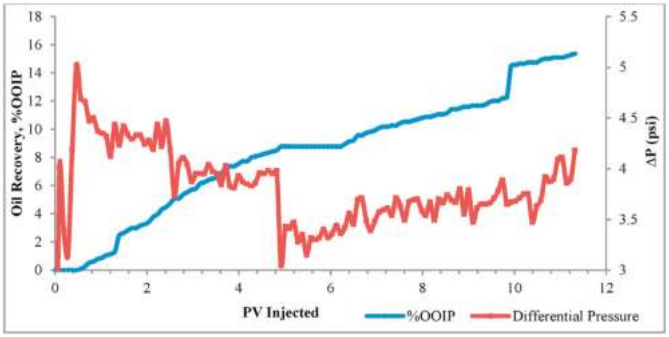

Fig. 26. CO_2 foam flooding using 2 wt% 15 nm nanosilica – 0.1 wt% TX100.

18.05% of OOIP. Pressure fluctuation was observed throughout the process which highly indicates the possibility of foam generation and degeneration (Hanssen and Dalland, 1990). Apparent viscosity measured is relatively low (0.002–0.0048 Pa s) than we expected for the foam stabilized with particles.

3.8.3. 2 wt% 15 nm nanosilica – 0.1 wt% TX100

At highly concentrated suspension, 2 wt% 15 nm nanosilica with similar TX100 concentration (Fig. 26), additional oil recovery recorded was 15.09% of OOIP. Pressure fluctuates at much higher range and significantly to generate estimated foams viscosity of with 0.0058–0.0096 Pa s. It is presumed that pressure different trends display the generation, degeneration and re-generation of CO_2 foams in porous media (Islam et al., 1989). Furthermore, it is speculated that gas mobility reduced due to the blocking effects, with high possibility of permeability reduction. The significant pressure different may possibly be contributed by nanosilica plugged in and off the pore throat, and propagate to the effluent (Spisak, 2011). Fig. 27 differentiates the oil produced during CO_2 foam flooding and waterflooding. The cloudy oil indicates the presence of nanosilica in the oil produced. However, it should be emphasized that some nanosilica – TX100 combinations recovered clear oil signifies particles retention in porous media.

Fig. 27. Cloudy (a) vs clear oil (b) produced during tertiary and secondary flooding, respectively.

3.8.4. 0.5 wt% 15 nm nanosilica – 0.5 wt% TX100

Excellent CO_2 foam stability obtained at 0.5 wt% 15 nm nanosilica - 0.5 wt% TX100 was further tested for EOR application. This combination results in 18.72% of OOIP being recovered. Apparent viscosity varies from 0.00359 to 0.01053 Pa s suggesting the strong CO_2 foams with fine textures, which was verified in earlier observation (Fig. 22A) (Apaydin et al., 1999; Li et al., 2012). Fig. 28 illustrates the recovery trend and pressure profile of the process. It is noticeable that, higher pressure drop ranges were recorded, giving higher estimated apparent foam viscosity.

3.8.5. 0.5 wt% 70 nm nanosilica – 0.01 wt% TX100

Although foam stability is high at 0.1 wt% TX100 with increasing nanosilica concentrations, injecting these combinations into the sandpack is impossible as the dispersions is heavily viscous, resulting in sandpack leaking due to higher pressure build up. Thus, we have eliminated several combinations at 0.1 wt% TX100 of 70 nm nanosilica to be tested for flooding experiment,

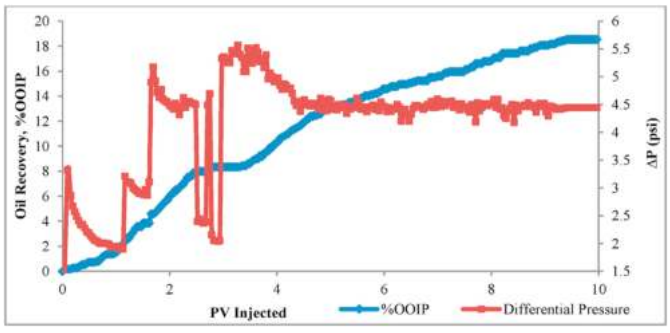

Fig. 28. CO_2 foam flooding using 0.5 wt% 15 nm nanosilica – 0.5 wt% TX100.

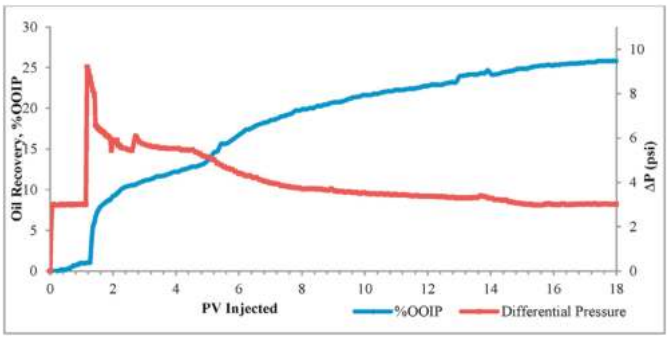

Fig. 29. CO_2 foam flooding using 0.5 wt% 70 nm nanosilica – 0.01 wt% TX100.

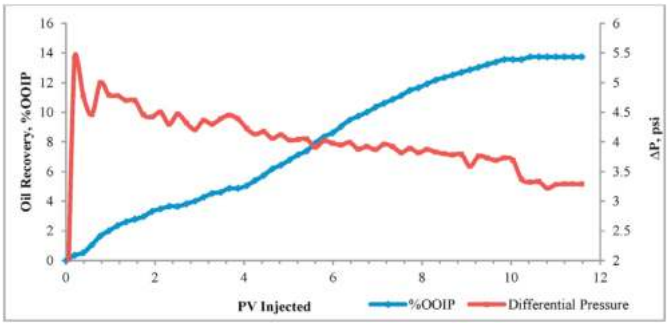

Fig. 30. CO_2 foam flooding using 1 wt% 70 nm nanosilica – 0.01 wt% TX100.

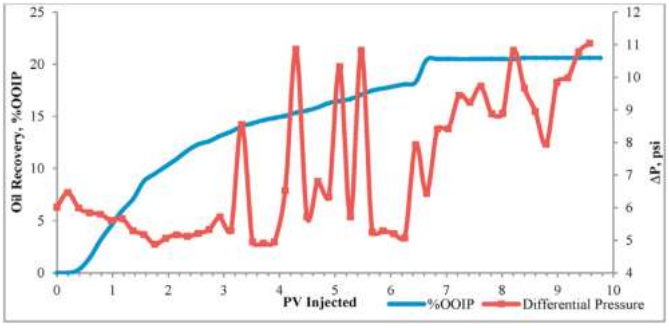

Fig. 31. CO_2 foam flooding using 7 wt% 70 nm nanosilica – 0.1 wt% TX100.

Nevertheless, foam flooding at 70 nm nanosilica at 0.5 wt% and 0.01 wt% TX100 was preformed, which lead to highest oil being produced, i.e, 22.27%. Fig. 29 shows the relevant plot. More fluids were continuously being injected as oil showing uninterrupted incremental recovery trend. Though sudden increase in pressure will theoretically lead in high apparent viscosity, rather, we suspected it is due to particles blockage in the porous media or typical pressure increased for foam generation. Pressure declined steadily afterwards with significant increase in oil recovery. Again, we concluded that this trend is reflected to finely textured bubbles generated in porous media as observed previously (Apaydin et al., 1999).

3.8.6. 1 wt% 70 nm nanosilica – 0.01 wt% TX100

Similar pressure trend as in section 3.8.5 was observed when 70 nm nanosilica fraction increased to 1 wt% (Fig. 30). Additional oil recovery however shows low increment, 13.74%.

3.8.7. 7 wt% 70 nm nanosilica – 0.1 wt% TX100

For this synergetic combination, the experiment was performed by alternately injecting the dispersion and CO_2 gases, i.e., SAG approaches. This was done as the concentrated dispersions unable to be injected via co-injection with CO_2 gases. For every 1 ml nanosilica – TX100 dispersion, CO_2 was injected at the same rate for 10 min to give equivalent foam quality produced as it is in earlier co-injecting procedures. Oil recovered reached 20.61% of OOIP with significant pressure fluctuation was observed. Pressure build-up was presumed to be primarily due to particles blockage as the dispersions is heavily saturated with silica particles. Fig. 31 shows the trend of oil recovery and pressure profile during the procedures.

From oil recovery experiments, nanosilica – TX100 combinations increased the amount of recoverable oil at least double the amount of oil recovered by conventional TX100 solution only as tabulated in Table 7. The trend however shows that, at constant TX100 concentrations, increasing nanosilica concentrations reduced the amount of oil recovered (Tests 2 and 3, and Tests 6 and 7). Nanosilica agglomeration was presumed to be the main factor where bigger particles might plug off porous media to retard fluid flow, hence reduced oil recovery. Tests 2, 4 and 6 are favorable for EOR application as optimum raw materials are required for high oil recovery.

Although the experiment was carried out at ambient conditions, it is highly expected that the combinations of nanosilica-TX100 would give remarkable outcomes at elevated pressure and temperature environment as being concluded in recent study by Yekeen et al. (2021b). The spherical shape of nanosilica and CO_2 foam quality were identified to have significant effect on foam stability at high temperature environment. Furthermore, optimum concentration of nanosilica at 0.5% yields maximum CO_2 foam stability implying its effectiveness at high pressure reservoir condition (Yekeen et al., 2021b). As much attention are focusing on the reservoir pressure and temperature condition for this EOR application, rather, studies suggested that nanoparticles shape and the their alignment and distribution at gas – liquid interface have more significant effect on CO_2 foam stability (Yekeen et al., 2021b; Zhang et al., 2021; Zhu et al., 2018). Despite that, the adsorption of TX100 molecules on nanosilica exhibits significant reduction at elevated temperature (Arain et al., 2020; Yekeen et al., 2021a), and thus further consideration on the amount of TX100 to be used need be highlighted should this combination were to be employed under reservoir condition as it may affect the nanosilica wettability and consequently the overall EOR process.

4. Conclusions

From this study, the following conclusions have been achieved.

(a) The in-situ physisorption of TX100 on both type of nanosilica did not turn the surface totally hydrophobic. Instead, the surfaces rendered partially hydrophobic, enable CO_2 foams stability.
(b) The 15 nm nanosilica-TX100 combinations show high CO_2 foams stability at intermediate TX100 concentrations, 0.1 and 0.5 wt%.
(c) Larger nanosilica in TX100 displays excellent CO_2 foam stability at lower surfactant concentration, mainly at 0.01 wt%.
(d) Nanosilica partitioning in CO_2 foam structure shows consistent relationships with that of contact angle measurements.
(e) Bubble sizes show insignificant relations with CO_2 foam stability.
(f) Synergetic performance of nanosilica and TX100 does facilitate CO_2 foam flooding, increasing oil recovery up to more than 20% of OOIP.

Table 7
CO_2 foam flooding experiment results.

TEST	1	2	3	4	5	6	7	8
SECONDARY RECOVERY (WATER FLOODING)								
Brine flowrate (ml/min)	0.50	0.50	0.50	0.50	0.50	0.50	0.50	0.50
PV injected	1.04	1.58	1.20	1.09	0.93	2.74	1.06	1.04
% Oil recovered	**52.25**	**51.10**	**52.63**	**56.61**	**54.22**	**44.53**	**54.87**	**52.12**
%Remaining oil in place	47.75	48.90	47.37	43.39	45.78	55.47	45.13	47.88
CO_2 FOAM FLOODING								
TX100 concentration, wt%	1.00	0.10	0.10	0.50	1.00	0.01	0.01	0.10
Nanosilica concentration, wt%	NA	0.10	2.00	0.50	0.10	0.50	1.00	7.00
Nanosilica sizes (nm)	NA	15	15	15	15	70	70	70
CO_2 flowrate (ml/min)	3.00	3.00	3.00	3.00	3.00	3.00	3.00	3.00
Dispersion flowrate (ml/min)	0.10	0.10	0.10	0.10	0.10	0.10	0.10	0.10
PV injected	13.20	10.00	10.00	10.00	10.00	10.00	10.00	9.77
Incremental recovery from CO_2 foam flooding (%)	**6.96**	**18.05**	**15.09**	**18.72**	**14.12**	**22.27**	**13.74**	**20.61**
% Total Recovery	**59.22**	**69.15**	**67.72**	**75.32**	**68.33**	**66.80**	**68.61**	**72.73**
Estimated foam apparent viscosity, Pa.s	0.0021 - 0.0044	0.002 - 0.0048	0.00582 - 0.0096	0.0036 - 0.011	0.0021- 0.0077	0.006 -0.0183	0.0064 - 0.011	0.010- 0.022

(g) For both nanosilica sizes at fixed TX100 concentration, increasing the concentrations was estimated to result in decreasing oil recovery.
(h) Other than foams generation, degeneration, and re-generation in the sandpack, pressure fluctuations during foam flooding indicates the occurrence of permeability changes during the flooding, enable CO_2 gases to flow in unpreferential path, further recovering trapped oil.

It should be emphasized that this experiment was performed at ambient conditions due to the lack in experimental setup availability. Hence, the uncertainties on the effect of pressure and temperature are expected. Future analysis on these effects should be evaluated to certain extent as CO_2 foam is anticipated to behave favorably at elevated pressure and temperature. Microscopic study should highly be considered to further observe and understand the mechanism of nanosilica partitioning at CO_2 – oil – water interfaces and their interaction.

Acknowledgement

Special thanks to Ministry of Higher Education, MOHE, Malaysia, Universiti Teknologi Malaysia, Johor Bahru, and Universiti Teknologi MARA, Shah Alam, for funding this research.

References

Adkins, S.S., Gohil, D., Dickson, J.L., Webber, S.E., Johnston, K.P., 2007. Water-in-carbon dioxide emulsions stabilized with hydrophobic silica particles. Phys. Chem. Chem. Phys. 9, 6333–6343.
Alkan, H., Goktekin, A., Satman, A., 1991. A Laboratory Study of CO2-Foam Process for Bati Raman Field, Turkey. Middle East Oil Show. Bahrain: Society of Petroleum Engineers.
Andrianov, A., Farajzadeh, R., Mahmoodi Nick, M., Talanana, M., Zitha, P.L.J., 2012. Immiscible foam for enhancing oil recovery: bulk and porous media experiments. Ind. Eng. Chem. Res. 51, 2214–2226.
Apaydin, O.G., Bertin, H., Castanier, L.M., Kovscek, A.R., 1999. An Experimental Investigation of Foam Flow in Homogeneous and Heterogeneous Porous Media. SUPRI TR-112, United States.
Arain, Z.-U.L.A., Al-Anssari, S., Ali, M., Memon, S., Bhatti, M.A., Lagat, C., Sarmadivaleh, M., 2020. Reversible and irreversible adsorption of bare and hybrid silica nanoparticles onto carbonate surface at reservoir condition. Petroleum 6, 277–285.
STM-D971-99a 2004. Standard Test Method for Interfacial Tension of Oil against Water by the Ring Method. ASTM International.
ASTM D 3519-88, R, 2007. Standard Test Method for Foam in Aqueous Media (Blender Test). ASTM International, Pennsylvania, USA.
Bai, B., 2008. Overview: EOR/IOR (january 2008). J. Petrol. Technol. 60, 42-42.
Bayat, A.E., Rajaei, K., Junin, R., 2016. Assessing the effects of nanoparticle type and concentration on the stability of CO2 foams and the performance in enhanced oil recovery. Colloid. Surface. Physicochem. Eng. Aspect. 511, 222–231.
Binks, B.P., 2002. Particles as surfactants—similarities and differences. Curr. Opin. Colloid Interface Sci. 7, 21–41.
Binks, B.P., Desforges, A., Duff, D.G., 2007. Synergistic stabilization of emulsions by a mixture of surface-active nanoparticles and surfactant. Langmuir 23, 1098–1106.
Binks, B.P., Horozov, T.S., 2005. Aqueous foams stabilized solely by silica nanoparticles. Angew. Chem. Int. Ed. 44, 3722–3725.
Binks, B.P., Murakami, R., Armes, S.P., Fujii, S., 2006. Effects of pH and salt concentration on oil-in-water emulsions stabilized solely by nanocomposite microgel particles. Langmuir 22, 2050–2057.
Blute, I., Pugh, R.J., van de Pas, J., Callaghan, I., 2007. Silica nanoparticle sols: 1. Surface chemical characterization and evaluation of the foam generation (foamability). J. Colloid Interface Sci. 313, 645–655.
Blute, I., Pugh, R.J., van de Pas, J., Callaghan, I., 2009. Industrial manufactured silica nanoparticle sols. 2: surface tension, particle concentration, foam generation and stability. Colloid. Surface. Physicochem. Eng. Aspect. 337, 127–135.
Borchardt, J.K., Bright, D.B., Dickson, M.K., Wellington, S.L., 1985. Surfactants for CO2 Foam Flooding.
Carn, F., Colin, A., Pitois, O., Vignes-Adler, M., Backov, R., 2009. Foam drainage in the presence of Nanoparticle–Surfactant mixtures. Langmuir 25, 7847–7856.
Chang, S.-H., Grigg, R.B., 1999. Effects of foam quality and flow rate on CO2-foam behavior at reservoir temperature and pressure. SPE Reservoir Eval. Eng. 2, 248–254.
Cui, Z.G., Cui, Y.Z., Cui, C.F., Chen, Z., Binks, B.P., 2010. Aqueous foams stabilized by in situ surface activation of CaCO3 nanoparticles via adsorption of anionic surfactant. Langmuir 26, 12567–12574.
Dellinger, S.E., Patton, J.T., Holbrook, S.T., 1984. CO2 mobility control. Soc. Petrol. Eng. J. 24, 191–196.
Dickinson, E., Ettelaie, R., Kostakis, T., Murray, B.S., 2004. Factors controlling the formation and stability of air bubbles stabilized by partially hydrophobic silica nanoparticles. Langmuir 20, 8517–8525.
Dong, X., Xu, J., Cao, C., Sun, D., Jiang, X., 2010. Aqueous foam stabilized by hydrophobically modified silica particles and liquid paraffin droplets. Colloid. Surface. Physicochem. Eng. Aspect. 353, 181–188.
Emrani, A.S., Ibrahim, A.F., Nasr-El-Din, H.A., 2017. Evaluation of mobility control with nanoparticle-stabilized CO2 foam. In: SPE Latin America and Caribbean Petroleum Engineering Conference. Society of Petroleum Engineers, Buenos Aires, Argentina.
Espinoza, D.A., Caldelas, F.M., Johnston, K.P., Bryant, S.L., Huh, C., 2010. Nanoparticle-stabilized supercritical CO2 foams for potential mobility control applications. In: SPE Improved Oil Recovery Symposium. Society of Petroleum Engineers, Tulsa, Oklahoma, USA.
Fan, X., Zhang, Z., Li, G., Rowson, N.A., 2004. Attachment of solid particles to air bubbles in surfactant-free aqueous solutions. Chem. Eng. Sci. 59, 2639–2645.
Fujii, S., Iddon, P.D., Ryan, A.J., Armes, S.P., 2006. Aqueous particulate foams stabilized solely with polymer latex particles. Langmuir 22, 7512–7520.
Fujii, S., Murakami, R., 2008. Smart particles as foam and liquid marble stabilizers. KONA Powder Particle J. 26, 153–166.
Giles, C.H., D'Silva, A.P., Easton, I.A., 1974a. A general treatment and classification of the solute adsorption isotherm part. II. Experimental interpretation. J. Colloid Interface Sci. 47, 766–778.
Giles, C.H., Smith, D., Huitson, A., 1974b. A general treatment and classification of the solute adsorption isotherm. I. Theoretical. J. Colloid Interface Sci. 47, 755–765.
Giordano-Palmino, F., Denoyel, R., Rouquerol, J., 1994. Interfacial aggregation of a nonionic surfactant: effect on the stability of silica suspensions. J. Colloid Interface Sci. 165, 82–90.
Gonzenbach, U.T., Studart, A.R., Tervoort, E., Gauckler, L.J., 2006. Tailoring the microstructure of particle-stabilized wet foams. Langmuir 23, 1025–1032.
Guignot, S., Faure, S., Vignes-Adler, M., Pitois, O., 2010. Liquid and particles retention in foamed suspensions. Chem. Eng. Sci. 65, 2579–2585.

Hanssen, J.E., Dalland, M., 1990. Foams for Effective Gas Blockage in the Presence of Crude Oil.
Haugen, A., Fernø, M.A.A., Graue, A., Bertin, H.J.J., 2012. Experimental study of foam flow in fractured oil-wet limestone for enhanced oil recovery. SPE Reservoir Eval. Eng. 15, 218–228.
Horozov, T.S., 2008. Foams and foam films stabilised by solid particles. Curr. Opin. Colloid Interface Sci. 13, 134–140.
Horozov, T.S., Binks, B.P., 2006. Particle-stabilized emulsions: a bilayer or a bridging monolayer? Angew. Chem. Int. Ed. 45, 773–776.
Hunter, T., Pugh, R., Franks, G., Jameson, G., 2008a. The role of particles in stabilising foams and emulsions. Adv. Colloid Interface Sci. 137, 57–81.
Hunter, T., Wanless, E., Jameson, G., Pugh, R., 2009a. Non-ionic surfactant interactions with hydrophobic nanoparticles: Impact on foam stability. Colloid. Surface. Physicochem. Eng. Aspect. 347, 81–89.
Hunter, T.N., Pugh, R.J., Franks, G.V., Jameson, G.J., 2008b. The role of particles in stabilising foams and emulsions. Adv. Colloid Interface Sci. 137, 57–81.
Hunter, T.N., Wanless, E.J., Jameson, G.J., Pugh, R.J., 2009b. Non-ionic surfactant interactions with hydrophobic nanoparticles: Impact on foam stability. Colloid. Surface. Physicochem. Eng. Aspect. 347, 81–89.
Islam, M.R., Selby, R.J., Ali, S.M.F., 1989. Mechanics of foam flow in porous media and applications. J. Can. Petrol. Technol. 28.
Ivanova, N.I., Volchkova, I.L., Shchukin, E.D., 1995. Adsorption of nonionic and cationic surfactants from aqueous binary mixtures onto the solid/liquid interface. Colloid. Surface. Physicochem. Eng. Aspect. 101, 239–243.
Karakashev, S.I., Ozdemir, O., Hampton, M.A., Nguyen, A.V., 2011. Formation and stability of foams stabilized by fine particles with similar size, contact angle and different shapes. Colloid. Surface. Physicochem. Eng. Aspect. 382, 132–138.
Kettlewell, S.L., Schmid, A., Fujii, S., Dupin, D., Armes, S.P., 2007. Is latex surface charge an important parameter for foam stabilization? Langmuir 23, 11381–11386.
Kruglyakov, P.M., Elaneva, S.I., Vilkova, N.G., 2011. About mechanism of foam stabilization by solid particles. Adv. Colloid Interface Sci. 165, 108–116.
Kruglyakov, P.M., Karakashev, S.I., Nguyen, A.V., Vilkova, N.G., 2008. Foam drainage. Curr. Opin. Colloid Interface Sci. 13, 163–170.
Ledakowicz, S., Perkowski, J., Bulska, A., Jamroz, T., Sencio, B., 2005. Ozonation Impact on degradation and toxicity of non-ionic surfactants. Ozone: Sci. Eng. 27, 437–445.
Levitz, P., Van Damme, H., 1986. Fluorescence decay study of the adsorption of nonionic surfactants at the solid-liquid interface. 2. Influence of polar chain length. J. Phys. Chem. 90, 1302–1310.
Levitz, P., Van Damme, H., Keravis, D., 1984. Fluorescence decay study of the adsorption of nonionic surfactants at the solid-liquid interface. 1. Structure of the adsorption layer on a hydrophilic solid. J. Phys. Chem. 88, 2228–2235.
Li, R.F., Hirasaki, G., Miller, C.A., Masalmeh, S.K., 2012. Wettability alteration and foam mobility control in a layered, 2D heterogeneous sandpack. SPE J. 17, 1207–1220.
Li, S., Li, Z., Wang, P., 2016. Experimental study of the stabilization of CO2 foam by sodium dodecyl sulfate and hydrophobic nanoparticles. Ind. Eng. Chem. Res. 55, 1243–1253.
Liu, Q., Zhang, S., Sun, D., Xu, J., 2009. Aqueous foams stabilized by hexylamine-modified Laponite particles. Colloid. Surface. Physicochem. Eng. Aspect. 338, 40–46.
Liu, Q., Zhang, S., Sun, D., Xu, J., 2010. Foams stabilized by Laponite nanoparticles and alkylammonium bromides with different alkyl chain lengths. Colloid. Surface. Physicochem. Eng. Aspect. 355, 151–157.
Okubo, T., 1995. Surface tension of structured colloidal suspensions of polystyrene and silica spheres at the air-water interface. J. Colloid Interface Sci. 171, 55–62.
Parida, S.K., Dash, S., Patel, S., Mishra, B.K., 2006. Adsorption of organic molecules on silica surface. Adv. Colloid Interface Sci. 121, 77–110.
Ravera, F., Santini, E., Loglio, G., Ferrari, M., Liggieri, L., 2006. Effect of nanoparticles on the interfacial properties of liquid/liquid and liquid/air surface layers. J. Phys. Chem. B 110, 19543–19551.
San, J., Wang, S., Yu, J., Liu, N., Lee, R., 2017. Nanoparticle-stabilized carbon dioxide foam used in enhanced oil recovery: effect of different ions and temperatures. SPE J. 22, 1416–1423.
Somasundaran, P., Snell, E.D., Xu, Q., 1991. Adsorption behavior of alkylarylethoxylated alcohols on silica. J. Colloid Interface Sci. 144, 165–173.
Spisak, B.J., 2011. Using Nanoparticle Stabilized Foam to Achieve Wellbore Stability in Shales.
Sun, Q., Li, Z., Li, S., Jiang, L., Wang, J., Wang, P., 2014. Utilization of surfactant-stabilized foam for enhanced oil recovery by adding nanoparticles. Energy Fuels 28, 2384–2394.
Tang, F.-Q., Xiao, Z., Tang, J.-A., Jiang, L., 1989. The effect of SiO2 particles upon stabilization of foam. J. Colloid Interface Sci. 131, 498–502.
Vijayaraghavan, K., Nikolov, A., Wasan, D., Henderson, D., 2009. Foamability of liquid particle suspensions: a modeling study. Ind. Eng. Chem. Res. 48, 8180–8185.
Worthen, A., Bagaria, H., Chen, Y., Bryant, S.L., Huh, C., Johnston, K.P., 2012. Nanoparticle stabilized carbon dioxide in water foams for enhanced oil recovery. In: SPE Improved Oil Recovery Symposium. Society of Petroleum Engineers, Tulsa, Oklahoma, USA.
Xu, X., Saeedi, A., Zhang, Y., Liu, K., 2016. Laboratory Investigation on CO2 Foam Flooding for Mature Fields in Western Australia.
Yekeen, N., Al-Yaseri, A., Idris, A.K., Khan, J.A., 2021a. Comparative effect of zirconium oxide (ZrO2) and silicon dioxide (SiO2) nanoparticles on the adsorption properties of surfactant-rock system: equilibrium and thermodynamic analysis. J. Petrol. Sci. Eng. 205, 108817.
Yekeen, N., Manan, M.A., Idris, A.K., Padmanabhan, E., Junin, R., Samin, A.M., Gbadamosi, A.O., Oguamah, I., 2018. A comprehensive review of experimental studies of nanoparticles-stabilized foam for enhanced oil recovery. J. Petrol. Sci. Eng. 164, 43–74.
Yekeen, N., Xin Kun, T., Al-Yaseri, A., Sagala, F., Kamal Idris, A., 2021b. Influence of critical parameters on nanoparticles-surfactant stabilized CO2 foam stability at sub-critical and supercritical conditions. J. Mol. Liq. 338, 116658.
Yusuf, S., Manan, M.A., Jaafar, M.Z., 2013. Aqueous Foams Stabilized by Hydrophilic Silica Nanoparticles via In-Situ Physisorption of Nonionic TX100 Surfactant.
Zeng, X., Osseo-Asare, K., 2004. Partitioning behavior of silica in the Triton X-100/dextran/water aqueous biphasic system. J. Colloid Interface Sci. 272, 298–307.
Zhang, S., Sun, D., Dong, X., Li, C., Xu, J., 2008. Aqueous foams stabilized with particles and nonionic surfactants. Colloid. Surface. Physicochem. Eng. Aspect. 324, 1–8.
Zhang, T., Roberts, M., Bryant, S.L., Huh, C., 2009. Foams and emulsions stabilized with nanoparticles for potential conformance control applications. In: SPE International Symposium on Oilfield Chemistry. Society of Petroleum Engineers, The Woodlands. Texas.
Zhang, X., Zhang, G., Ge, J., Wang, Y., 2020. CO foam stabilized with switchable surfactants and modified nanoparticles effected by PH and salinity. In: SPE Europec. Society of Petroleum Engineers, Amsterdam, The Netherlands.
Zhang, Y., Liu, Q., Ye, H., Yang, L., Luo, D., Peng, B., 2021. Nanoparticles as foam stabilizer: mechanism, control parameters and application in foam flooding for enhanced oil recovery. J. Petrol. Sci. Eng. 202, 108561.
Zhang, Y., Xu, G., Bo, H., Li, X., 2014. Foam Flooding Technology Used for Enhanced Oil Recovery in Offshore Oilfields of China's Bohai Bay.
Zhao, J., Torabi, F., Yang, J., 2021. The synergistic role of silica nanoparticle and anionic surfactant on the static and dynamic CO2 foam stability for enhanced heavy oil recovery: an experimental study. Fuel 287, 119443.
Zhu, J., Yang, Z., Li, X., Wang, Z., Lu, Y., 2018. Synergistic Effect between Wormlike Micelles and Nanoparticles in Stabilizing Foams for High Temperature Stimulation.
Zhu, Y., Hou, Q., Weng, R., Jian, G., Luo, Y., Li, J., 2013. Recent Progress and Effects Analysis of Foam Flooding Field Tests in China.
Zhu, Y., Tian, J., Hou, Q., Luo, Y., Fan, J., 2017. Studies on nanoparticle-stabilized foam flooding EOR for a high temperature and high salinity reservoir. In: Abu Dhabi International Petroleum Exhibition & Conference. Society of Petroleum Engineers, Abu Dhabi, UAE.
Zhuravlev, L.T., 2000. The surface chemistry of amorphous silica. Zhuravlev Model. Colloids Surfaces A: Physicochem. Eng. Aspects 173, 1–38.
Zuidema, H., Waters, G., 1941. Ring method for the determination of interfacial tension. Indus. Eng. Chem. Anal. Ed. 13, 312–313.